Soft Matter

PAPER

View Article Online
View Journal | View Issue

Cite this: *Soft Matter*, 2024, **20**, 3676

Deformation-dependent gel surface topography due to the elastocapillary and osmocapillary effects†

Luochang Wang and Qihan Liu *

Received 28th January 2024,
Accepted 11th April 2024

DOI: 10.1039/d4sm00139g

rsc.li/soft-matter-journal

Actively tuning surface topography is crucial for the design of smart surfaces with stimuli-responsive friction, wetting, and adhesion properties. This paper studies how elastocapillary deformation and osmocapillary phase separation can lead to rich deformation-dependent surface topography in polymeric gels. In a purely elastic material, stretching always flattens the surface due to the Poisson effect. We show that stretching can roughen the surface due to the elastocapillary and osmocapillary effects. The roughening can be tuned by the gel stiffness, the gel osmotic pressure, the deformation mode, and the initial amplitude of surface roughness. The rich deformation-dependent behavior of gel surface topography points to a new direction in designing smart surfaces.

1. Introduction

Surface topography governs many surface behaviors such as friction, wetting, adhesion, and transparency.[1–7] Smart surfaces that actively control surface behavior through surface topography have been extensively studied. For example, swelling a polymeric gel expands surface features,[8–12] and stretching a soft material deforms the surface topography with the bulk.[13–17] Although deforming a piece of material is simple, predicting the deformation-dependent surface topography is not.[12,14,18] By elastic deformation alone, stretching the material flattens surface topography due to the Poisson effect. However, if the material is sufficiently soft, surface tension can deform the surface topography, causing elastocapillary deformation.[14,17–22] If the material is sufficiently swollen with a solvent, surface tension can pull the solvent out from the material bulk, leading to osmocapillary phase separation.[12,23–25] While the elastocapillary and osmocapillary effects on a static surface are relatively well studied, how they affect surface topography during deformation remains unclear. Understanding the deformation-dependent elastocapillary and osmocapillary effects is crucial to predicting the deformation-dependent surface topography and designing novel smart surfaces.

In general, a deformation can be decomposed into a volumetric and an incompressible part. This paper focuses on the surface topography change under incompressible deformation. The change under volumetric deformation have been recently reported.[12] We perform novel finite element simulation that incorporates coupled elastocapillary and osmocapillary effects. We use a sinusoidal profile to reveal the length dependence of the elastocapillary and osmocapillary effects. The simulation shows that the elastocapillary and osmocapillary effects can lead to non-monotonic surface roughening and flattening with deformation. Here roughening or flattening means an increase or decrease in the amplitude of surface undulation. The findings point to new possibilities to program complex surface responses. Our findings also echo a recent experimental study that found PDMS gels can either roughen or flatten under stretch depending on the elastic moduli.[14] The paper attributed the observation to strain-dependent surface tension and elastocapillary deformation alone. Our study shows that similar phenomena could happen under constant surface tension when both the elastocapillary and osmocapillary effects are considered.

2. Governing mechanisms for the deformation-dependent gel surface topography

A polymeric gel consists of a polymer network infiltrated with a solvent. The polymer network leads to a solid-like elastic behavior;[26] the solvent leads to a liquid-like capillary behavior, which dominates the gel surface at high solvent content;[27] and the absorption of the solvent by the polymer network leads to an osmotic behavior.[28] In the absence of external load, the gel surface topography is governed by the competition between elasticity, capillarity, and osmosis. Elasticity resists any deformation thus maintaining the stress-free surface topography.

Department of Mechanical Engineering and Materials Science, University of Pittsburgh, Pittsburgh, PA 15213, USA. E-mail: qihan.liu@pitt.edu

† Electronic supplementary information (ESI) available. See DOI: https://doi.org/10.1039/d4sm00139g

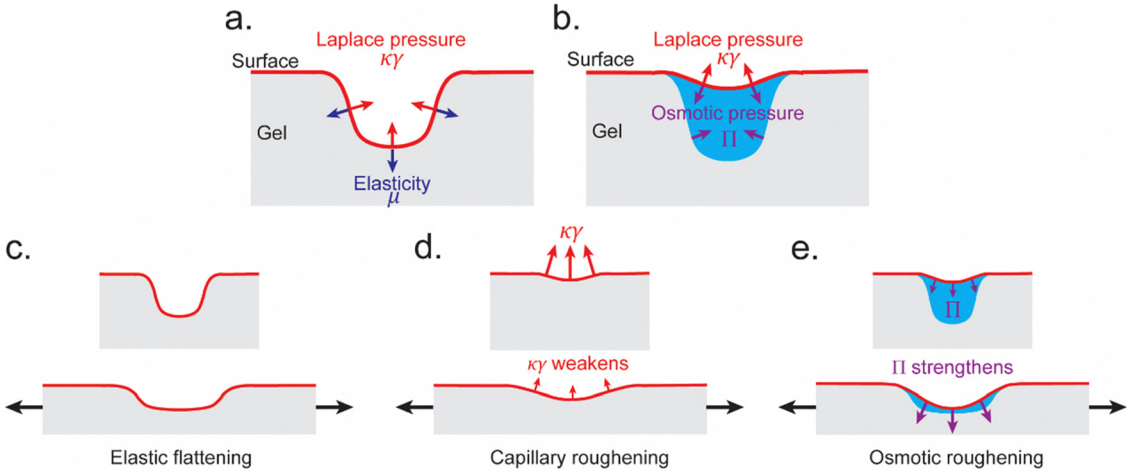

Fig. 1 (a) The competition between elasticity and capillarity results in elastocapillary deformation. (b) The competition between osmosis and capillarity results in osmocapillary phase separation. (c) Elasticity leads to surface flattening under stretch. (d) Capillarity is weakened by the lower curvature under stretch, thus roughening the surface. (e) Osmosis is strengthened by the tensile hydrostatic stress that increases Π under stretch, thus roughening the surface.

Capillarity tends to minimize the surface area by flattening the surface topography. The competition between elasticity and capillarity to deform the polymer network is known as elastocapillary deformation (Fig. 1a).[20] Here capillarity is governed by the Laplace pressure $\gamma\kappa$, where γ is surface energy and κ is the sum of the two principal curvatures of the surface. Elasticity is governed by the shear modulus μ of the gel. The elastocapillary effect is governed by the dimensionless number $\gamma\kappa/\mu$, where $\gamma\kappa \gg \mu$ leads to significant elastocapillary deformation. On the other hand, osmosis absorbs the solvent that covers surface asperities thus roughening the surface topography. The competition between osmosis and capillarity to move the surface solvent is known as osmocapillary phase separation (Fig. 1b).[23] Here osmosis is governed by the osmotic pressure Π. The osmocapillary effect is governed by the dimensionless number $\gamma\kappa/\Pi$, where $\gamma\kappa \gg \Pi$ leads to significant osmocapillary phase separation. Due to the elastocapillary and osmocapillary effects, the equilibrium surface topography generally deviates from the stress-free surface topography.

When the gel is externally loaded, elasticity, osmosis, and capillarity respond to the deformation differently. Consider a uniform stretch (Fig. 1c). Elasticity elongates the surface topography with the gel bulk and the Poisson effect flattens the surface. The elongation of the surface topography decreases the surface curvature κ. Consequently, the Laplace pressure $\gamma\kappa$ that flattens the surface is reduced, and the surface roughens (Fig. 1d). On the other hand, the tensile stress during stretch increases the osmotic pressure Π that resists phase separation.[29] Consequently, the volume of solvent between asperity reduces, which also roughens the surface (Fig. 1e). The competition between elasticity, capillarity, and osmosis evolves with deformation, which can lead to complex deformation-dependent surface topography.

3. Finite element simulation of coupled elastocapillary and osmocapillary effects

This paper uses finite element simulation to study the coupled elastocapillary and osmocapillary effects in deformation-dependent surface topography. The elastocapillary and osmocapillary effects are characterized by elastocapillary length γ/μ and osmocapillary length γ/Π.[20,23] To cleanly study the length dependence of the elastocapillary and osmocapillary effects, we study a sinusoidal surface profile, which only involves two length scales, the wavelength L_0 and the peak-to-peak

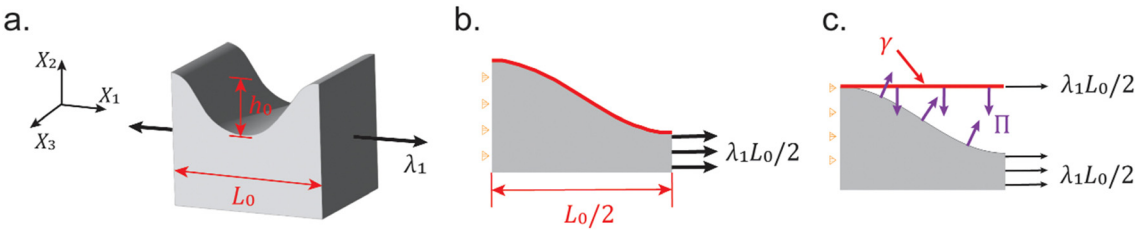

Fig. 2 (a) We study the evolution of a sinusoidal profile under uniform deformation. (b) Thanks to the symmetry and periodicity, only half a period in 2D needs to be simulated. (c) The surface is simulated as a beam with pretension that matches the surface tension γ pulled towards the gel by the osmotic pressure Π.

amplitude h_0 in the stress-free state (Fig. 2a). Then the equilibrium surface amplitude h without external load is completely determined by three dimensionless numbers:

$$\frac{h}{L_0} = F\left(\frac{\gamma}{\mu L_0}, \frac{\gamma}{\Pi L_0}, \frac{h_0}{L_0}\right). \quad (1)$$

When the gel is uniformly deformed, the deformation is governed by the principle stretches, $\lambda_1,\lambda_2,\lambda_3$. For incompressible deformation, $\lambda_1\lambda_2\lambda_3 = 1$, only two stretches are independent. Take λ_1 along the direction of the sinusoidal wave and λ_2 along the direction perpendicular to the surface (Fig. 2a), the deformation-dependent surface amplitude change can be written as:

$$\frac{h(\lambda_1)}{h_0} = G\left(\lambda_1; \frac{\gamma}{\mu L_0}, \frac{\gamma}{\Pi L_0}, \frac{h_0}{L_0}, \lambda_3\right). \quad (2)$$

We perform finite element simulation to investigate the effects of each of the four dimensionless numbers in eqn (2).

A commercial finite element package, ABAQUS, is used for the simulation. We perform all simulations in the plane strain condition ($\lambda_3 = 1$), then transform the results to generalized plane strain conditions with different λ_3.[30,31] Due to the symmetry and periodicity of a sinusoid, we only model half a period (Fig. 2b). We consider the common case that the surface amplitude is much smaller than the sample thickness and set the gel thickness is to be larger than $50h_0$. Then the bottom boundary negligibly affects the simulation. The gel bulk is modeled with neo-Hookean elasticity. 2D quadratic hybrid plane-strain element, CPE8H, is used to discretize the simulation domain. We only study the equilibrium state after the complete poroelastic relaxation. Consequently, there is no solvent flux, and the osmotic pressure is uniform everywhere. On the other hand, since the gel modulus depends on the solvent content,[32] the near-surface solvent migration can lead to spatial variation in the gel modulus. For common low-roughness surfaces, the deformation and solvent migration to flatten the asperities are small. Consequently, we neglect the deformation-dependent gel modulus in the current study.

The gel surface is modeled with a layer of quadratic beam elements, B22. We ensure the beam behaves like the surface tension through three features:[31] (1) a uniform prestress is applied so that the tension in the beam matches the surface tension γ, (2) the tensile stiffness of the beam is so low that the deformation in the simulation negligibly affects the prestress and the cross-section Poisson's ratio is set to 0 so that deformation does not change the cross-section area. Then surface tension γ is independent of deformation. (3) The bending stiffness of the beam is so low that the beam layer negligibly affects the deformation of the gel. For simplicity, we assume the surface tension of the gel is identical to that of the solvent, which is valid for gels of high solvent content.[12,27] In gels of low solvent content, the gel surface stress can be different from the solvent surface tension and can be strain-dependent.[14,33,34]

To simulate coupled elastocapillary deformation and osmocapillary phase separation, the beam and the gel are pulled towards each other by a uniform pressure that matches the magnitude of the osmotic pressure Π (Fig. 2c). The "hard contact" interaction in ABAQUS is used to prevent the beam from penetrating the gel. We model the deformation-dependent osmotic pressure Π using the incompressible neo-Hookean model:[29]

$$\sigma_2 = \mu(\lambda_2^2 - 1) - \Pi_0 + \Pi. \quad (3)$$

Here Π_0 and Π are the initial and current osmotic pressure. Assuming the surface is stress-free, $\sigma_2 = 0$ and recall the incompressibility constraint $\lambda_1\lambda_2\lambda_3 = 1$, we have:

$$\Pi = \Pi_0 - \mu\left(\frac{1}{\lambda_1^2\lambda_3^2} - 1\right). \quad (4)$$

The incompressible neo-Hookean law is valid to derive the osmotic pressure change because (1) we assume the amplitude of the surface topography is much smaller than the thickness of the gel. Consequently, osmocapillary phase separation on the surface negligibly affects the bulk solvent content. And (2) we neglect solvent evaporation from the gel surface. The local deformation near the surface can be compressible due to solvent migration. We will first study the incompressible case in Sections 4 and 5 and discuss the effect of compressibility in Section 6.

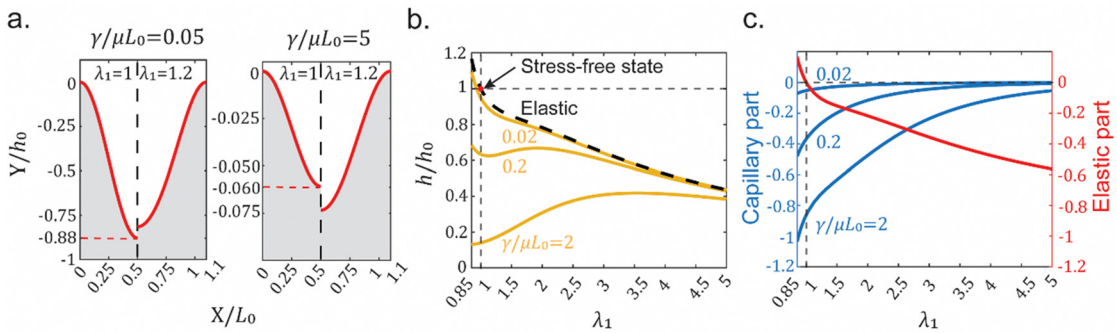

Fig. 3 (a) Surface flattens with stretch when elasticity dominates over capillarity and roughens with stretch when capillarity dominates over elasticity. (b) Surface roughens with stretch for large $\gamma/\mu L_0$ and small tensile stretch λ_1. (c) Elasticity monotonically flattens while capillarity monotonically roughens the surface with stretch.

4. The elastocapillary effect: $\gamma/\mu L_0$

When osmotic pressure Π is sufficiently large ($\gamma/\Pi_0 L_0 \ll 1$), the solvent will be completely absorbed into the gel bulk. Then there is no osmocapillary phase separation. Elastocapillary deformation alone determines the deformation-dependent surface topography. Consider a fixed $h_0/L_0 = 0.2$ under plane strain deformation, eqn (2) simplified to $h/h_0 = G(\lambda_1;\gamma/\mu L_0)$, which can be easily studied by simulating a group of $h(\lambda_1)/h_0$ curves with various $\gamma/\mu L_0$. Our simulations show that when the capillary effect is weak ($\gamma/\mu L_0 < 1$, Fig. 3a), the surface is little deformed before stretching (left half of the subfigure with $h/h_0 = 0.88$) and stretching the surface leads to flattening. This is expected from the Poisson effect. When the capillary effect is strong ($\gamma/\mu L_0 > 1$, Fig. 3a), the surface is significantly flattened before stretching (left half of the subfigure with $h/h_0 = 0.06$), and stretching the surface roughens the surface. This is because the capillary flattening is weakened.

To quantitatively illustrate the deformation-dependent surface flattening in Fig. 3a, we plot $h/h_0 = G(\lambda_1;\gamma/\mu L_0)$ in Fig. 3b. It shows that a larger $\gamma/\mu L_0$ results in more significant surface flattening (smaller h/h_0) at all stretch levels. When the capillary effect is weak ($\gamma/\mu L_0 = 0.02$), the surface monotonically flattens with stretch (decreasing h/h_0) similar to an elastically deformed surface. However, when the capillary effect is strong ($\gamma/\mu L_0 = 0.2$ or 2), the surface roughens with stretch for small deformation (increasing h/h_0 for λ_1 near 1), then flattens with stretch for large deformation (λ_1 far from 1, either tensile or compressive). The range of roughening behavior broadens as $\gamma/\mu L_0$ increases. We do not simulate $\lambda_1 < 0.85$ because a crease forms at the bottom of the trough. Crease-induced surface topography change is a different topic that we will not investigate. Readers may refer to existing ref. 30, 31 and 35.

The non-monotonic behavior can be interpreted as the competition between the elastic flattening and capillary roughening. To separate the elastic and capillary contributions on the surface deformation, we divide the total change in surface profile amplitude, $h - h_0$, into two parts: the capillary part $h - h_e$ and the elastic part $h_e - h_0$. Here h_e is the stretch-dependent surface profile amplitude without capillary effect (*i.e.*, $\gamma/\mu L_0 = 0$). Then $h_e - h_0$ represents the contribution due to elastic deformation, and $h - h_e$ represents the additional deformation induced by capillarity. Fig. 3c shows that elastic flattening due to the Poisson effect strengthens monotonically with stretch in both tensile ($h_e - h_0 < 0$) and compressive ($h_e - h_0 > 0$) directions. In contrast, the capillary flattening weakens monotonically with stretch in the tensile direction (approaches 0) because stretching reduces the local curvature. For small $\gamma/\mu L_0$, the elastic part dominates over the capillary part at any stretch λ_1 (the absolute value of the red curve dominates over the blue curves), leading to monotonically flattening with stretch. For larger $\gamma/\mu L_0$, the capillary part dominates over the elastic part for small deformation (λ_1 near 1), leading to stretch-dependent roughening. However, the elastic part still dominates over the capillary part for large deformation (λ_1 far from 1), leading to stretch-dependent flattening.

5. Osmocapillary effect: $\gamma/\Pi_0 L_0$

When osmotic pressure is sufficiently small, the solvent can be pulled out from the gel bulk by capillarity, leading to osmocapillary phase separation.[23] Deforming the gel bulk impacts osmocapillary phase separation in two ways: (1) stretching the surface reduces the local curvature thus weakening the capillary effect, and (2) tensile stress increases the osmotic pressure thus strengthening the osmotic effect. Since both the weakening of the capillary effect and the strengthening of the osmotic effect roughen the surface, stretching always roughens the surface in the presence of osmocapillary phase separation (Fig. 4a). Since both effects reduce the amount of osmocapillary phase separation, there exists a critical λ_{dry} where osmocapillary phase separation disappears for $\lambda_1 > \lambda_{dry}$. Then the surface deformation is purely elastocapillary, which has been discussed in Section 4. Based on the same argument, compression increases the amount of osmocapillary phase separation. There exists a critical λ_{wet} where $\Pi = 0$ and the solvent is squeezed out of the surface. When the solvent completely covers the surface, the liquid surface is completely flattened by capillarity.

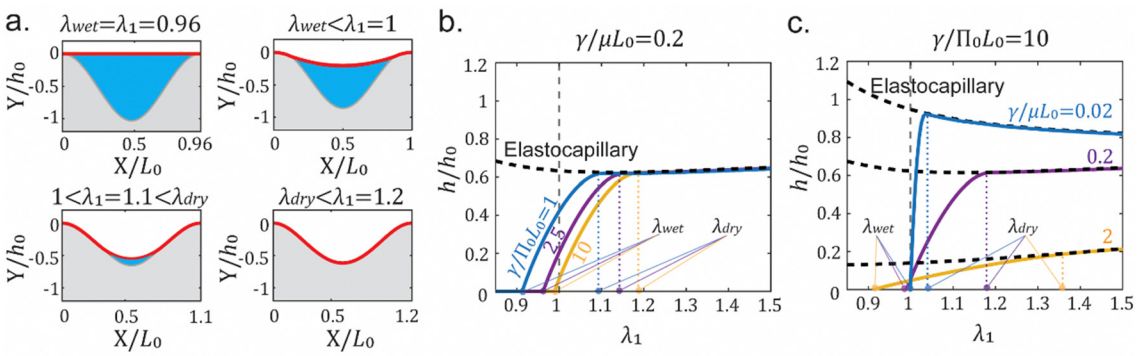

Fig. 4 (a) Under plane strain condition, osmocapillary phase separation reduces with stretch. Osmocapillary phase separation disappears for $\lambda_1 > \lambda_{dry}$ and inundate the surface for $\lambda_1 < \lambda_{wet}$. Here $\gamma/\mu L_0 = 0.2$, $\gamma/\Pi_0 L_0 = 2.5$. (b) Under a fixed $\gamma/\mu L_0$, a larger $\gamma/\Pi_0 L_0$ shifts λ_{dry} and λ_{wet} to larger stretches. (c) Under a fixed $\gamma/\Pi_0 L_0$, a larger $\gamma/\mu L_0$ flattens the surface and widen the gap between λ_{dry} and λ_{wet}.

The deformation-dependent osmocapillary phase separation in Fig. 4a is governed by two dimensionless numbers, the same elastocapillary number $\gamma/\mu L_0$, and the osmocapillary number $\gamma/\Pi_0 L_0$. We first plot $h(\lambda_1)/h_0$ with the fixed $\gamma/\mu L_0 = 0.2$ and varying $\gamma/\Pi_0 L_0$ (Fig. 4b). It shows that a larger $\gamma/\Pi_0 L_0$ corresponds to a larger amount of initial osmocapillary phase separation at $\lambda_1 = 1$ and shifts both λ_{dry} and λ_{wet} to larger stretches (Fig. S2a, ESI†). The surface roughness is independent of $\gamma/\Pi_0 L_0$ once phase separation disappears ($\lambda_1 > \lambda_{dry}$) or inundates the surface ($\lambda_1 < \lambda_{wet}$). Next, we plot $h(\lambda_1)/h_0$ with fixed $\gamma/\Pi_0 L_0 = 10$ and varying $\gamma/\mu L_0$ (Fig. 4c). It shows two trends: (1) a larger γ implies stronger elastocapillary flattening, thus lowering h/h_0 when the surface is stretched ($\lambda_1 > 1$). (2) According to eqn (4), a smaller μ results in a weaker stretch dependence of Π, thus a larger gap between λ_{dry} and λ_{wet} (Fig. S2b, ESI†).

6. The effect of Poisson's ratio

The two above sections illustrate the competition between the stretch-induced flattening caused by the Poisson effect and the stretch-induced roughening caused by elastocapillary and osmocapillary effects. So far, we have assumed the polymer network to be incompressible with a Poisson's ratio $\nu = 0.5$. In general, the Poisson's ratio of a gel depends on the swelling ratio, as can be illustrated by the Flory–Rehner model (Section S3, ESI†). According to the Flory–Rehner model, polymer networks are nearly incompressible, *i.e.* shear is much easier than volumetric deformation, in most conditions even if free solvent exchange is allowed (Fig. S3, ESI†). This contradicts with much lower Poisson's ratios measured through some indentation tests.[36–39] Such contradictions are expected because the Flory–Rehner model has been shown to severely underestimate the volumetric elasticity of the polymer network.[40] In the lack of an accurate compressible constitutive model for polymer networks, here we use the classical compressible neo-Hookean model to qualitatively illustrate the effect of network compressibility.[41] We tune the Poisson's ratio between $\nu = 0$ to 0.5 and repeat the simulations for the elastocapillary and osmocapillary cases. Since the Poisson effect is responsible for the stretch-induced flattening and the capillary effect is responsible for the stretch-induced roughening, lowering the Poisson ratio will reduce the flattening effect. In the limit of $\nu = 0$, the surface will monotonically roughen with stretch (Fig. 5a). On the other hand, a lower Poisson's ratio makes the gel more deformable under surface tension, thus rendering the surface flatter before stretching. The flatter surface makes osmocapillary phase separation easier to absorb, thus lowering λ_{dry} (Fig. 5b).

7. The effect of out-of-plane deformation: λ_3

So far, we have been concerned with the plane strain deformation where $\lambda_3 = 1$. The results of plane strain deformation can be transformed into any generalized plane strain deformation with a uniform $\lambda_3 \neq 1$.[30,31] We derive the transformation for osmocapillary phase separation as follows (Fig. 6). We take the reference state as the stress-free state with no surface energy, thus no elastocapillary deformation or osmocapillary phase separation. After applying a macroscopic plane strain stretch and relaxing the surface under surface tension γ and osmotic pressure Π, the bulk material will have an inhomogeneous field of $\boldsymbol{F}^{(PE)}$ and there will be some osmocapillary phase separation. Consider a unit thickness of material in the reference state, the free energy after deformation is:

$$W_{PE} = \iint_{bulk} \frac{\mu}{2} F^{(PE)}_{\alpha\beta} F^{(PE)}_{\alpha\beta} \mathrm{d}X_1 \mathrm{d}X_2 + \gamma S + \Pi A + \text{const.} \quad (5)$$

Here $\alpha,\beta = 1, 2$. The first integration integrates over the deformation plane. S is the length of the surface in the deformation plane, and A is the area of phase separation in the deformation plane.

Consider the same piece of material undergoes a generalized plane strain deformation. The total deformation of the gel can be decomposed into a uniaxial deformation $\boldsymbol{F}^{(UA)}$ followed by a plane strain deformation $\boldsymbol{F}^{(PE)}$, $\boldsymbol{F}^{(GPE)} = \boldsymbol{F}^{(PE)}\boldsymbol{F}^{(UA)}$. We assume the uniaxial deformation is uniform with no capillary effect. Then the following plane strain deformation relative to

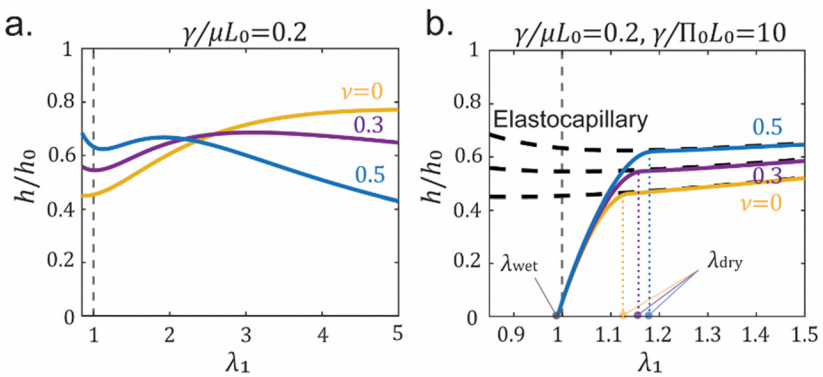

Fig. 5 (a) A lower Poisson's ratio decreases elastic effect, thus flattening the surface at the undeformed state and suppresses the stretch-induced flattening. (b) A lower Poisson's ratio flattens surface at smaller stretch, thus shifting λ_{dry} to a smaller stretch.

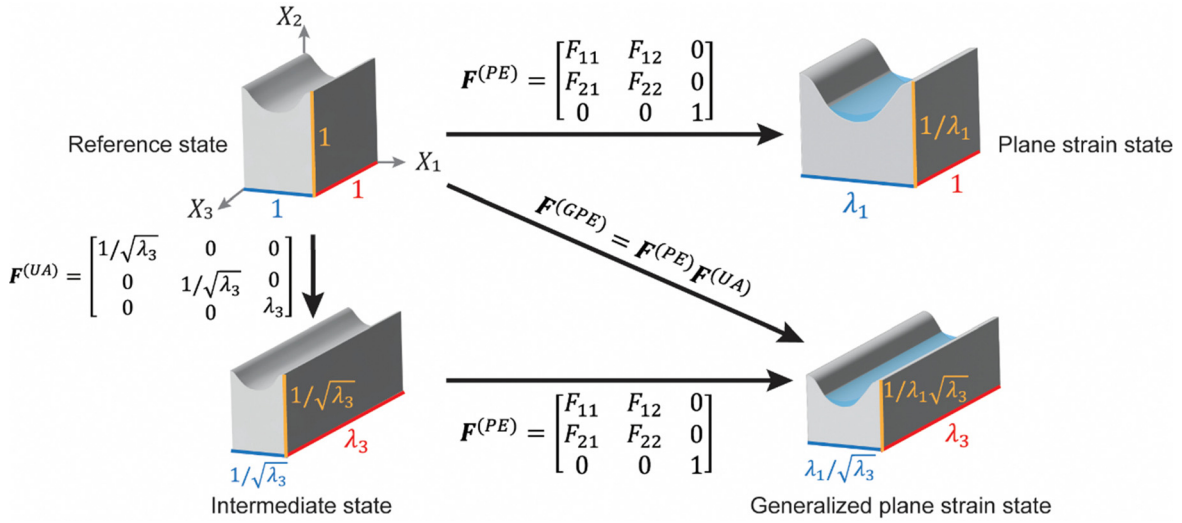

Fig. 6 A generalized plane strain deformation (GPE) can be decomposed into a uniaxial deformation (UA) followed by a plane strain deformation (PE).

the intermediate state is governed by the same physics as the plane strain deformation relative to the reference state discussed above. The only difference is that after $\boldsymbol{F}^{(\mathrm{UA})}$, the unit thickness in the reference state elongates to λ_3 in the intermediate state and any in-plane dimension in the intermediate state is shrunk by compared to the reference state. Then eqn (5) should be modified as:

$$W_{\mathrm{GPE}} = \iint_{\mathrm{bulk}} \frac{\mu}{2\lambda_3} F_{\alpha\beta}^{(\mathrm{PE})} F_{\alpha\beta}^{(\mathrm{PE})} \mathrm{d}X_1 \mathrm{d}X_2 + \lambda_3 \left[\gamma \frac{S}{\sqrt{\lambda_3}} + \Pi \frac{A}{\lambda_3} \right] + f(\lambda_3). \tag{6}$$

The last term $f(\lambda_3)$ involves a few terms that depend on λ_3 but not the in-plane deformation or phase separation. Since λ_3 is a constant during the generalized plane strain deformation, $f(\lambda_3)$ is a constant that can be dropped from the analysis. Comparing eqn (5) and (6), we see that the energy minimization of W_{GPE} with $\mu^{(\mathrm{GPE})}$, $\gamma^{(\mathrm{GPE})}$, $\Pi^{(\mathrm{GPE})}$ under a macroscopic stretch $\lambda_1^{(\mathrm{GPE})}$ is equivalent to the energy minimization of W_{PE} with $\mu^{(\mathrm{PE})}$, $\gamma^{(\mathrm{PE})}$, $\Pi^{(\mathrm{PE})}$ under a macroscopic stretch $\lambda_1^{(\mathrm{PE})}$ through the following transformation:

$$\begin{cases} \mu^{(\mathrm{PE})} = \mu^{(\mathrm{GPE})}/\lambda_3, \\ \gamma^{(\mathrm{PE})} = \sqrt{\lambda_3}\gamma^{(\mathrm{GPE})}, \\ \Pi^{(\mathrm{PE})} = \Pi^{(\mathrm{GPE})}, \\ \lambda_1^{(\mathrm{PE})} = \sqrt{\lambda_3}\lambda_1^{(\mathrm{GPE})}. \end{cases} \tag{7}$$

Here $\lambda_1^{(\mathrm{PE})} = \sqrt{\lambda_3}\lambda_1^{(\mathrm{GPE})}$ directly follows from $\boldsymbol{F}^{(\mathrm{GPE})} = \boldsymbol{F}^{(\mathrm{PE})}\boldsymbol{F}^{(\mathrm{UA})}$.

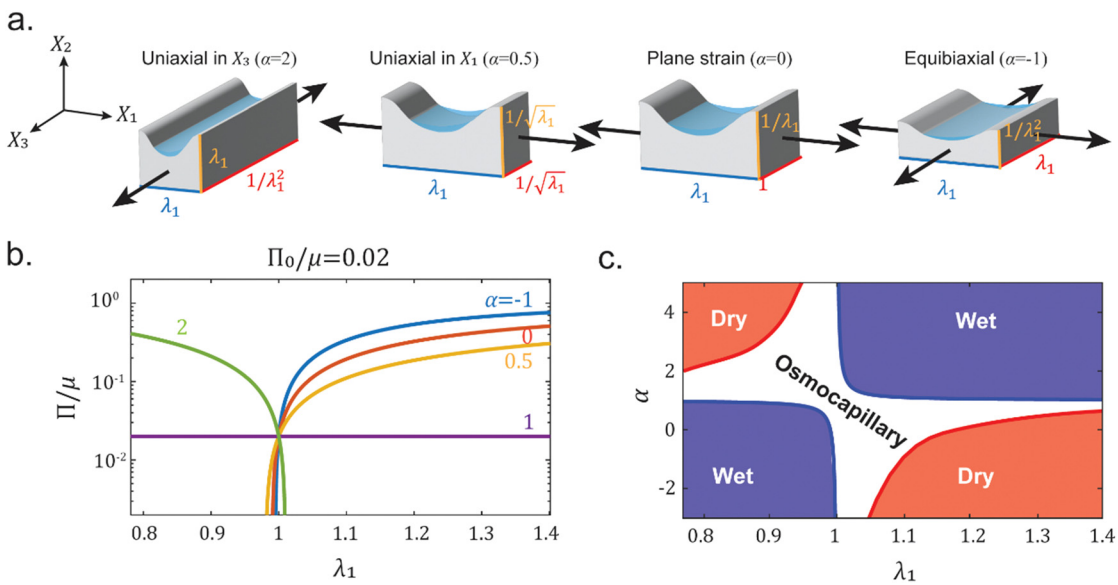

Fig. 7 (a) Various deformation modes and the corresponding α in the constraint $\lambda_3 = 1/\lambda_1^{\alpha}$. (b) α affects the $\Pi - \lambda_1$ dependence. (c) The phase diagram of the surface states. "Dry", "osmocapillary", and "wet" mean none, partial, and complete solvent coverage of the surface. Here $\gamma/\Pi_0 L_0 = 10$, $\gamma/\mu L_0 = 0.2$.

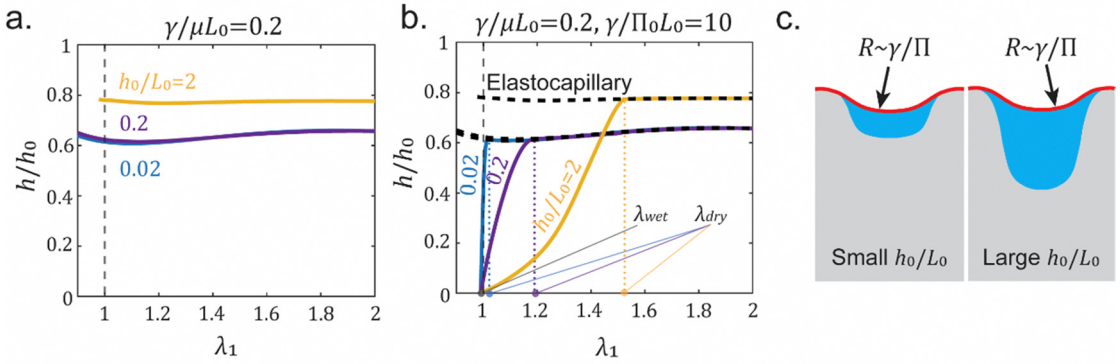

Fig. 8 (a) Elastocapillary deformation is independent of amplitude for shallow surface with $h_0/L_0 \ll 1$ and causes less flattening for $h_0/L_0 > 1$. (b) Osmocapillay phase separation extends to higher stretches with larger surface amplitude h_0/L_0. (c) A Larger amplitude leads to a larger amount of osmocapillary phase separation.

The transformation eqn (7) allows us to study various loading conditions with arbitrary λ_3. Most common loading conditions can be represented by the relation $\lambda_3 = 1/\lambda_1^{\alpha}$. For example, $\alpha = 0$ corresponds to the plane strain deformation ($\lambda_3 = 0$) and $\alpha = -1$ corresponds to equibiaxial deformation ($\lambda_3 = \lambda_1$). Fig. 7a lists a few common deformation modes and their corresponding α. In these cases, eqn (4) becomes:

$$\Pi = \Pi_0 - \mu\left(\frac{1}{\lambda_1^{2-2\alpha}} - 1\right). \quad (8)$$

Eqn (8) implies that the larger the α, the slower the Π increases with λ_1; Π is deformation independent when $\alpha = 1$; and Π decreases with λ_1 for $\alpha > 1$, (Fig. 7b). As discussed in Fig. 4c, the deformation-dependent Π governs the gap between λ_{dry} and λ_{wet}. For an incompressible network with fixed $\gamma/\Pi_0 L_0 = 10$, $\gamma/\mu L_0 = 0.2$, we have performed generalized plane strain simulations for various α. The result can be represented by a phase diagram of the surface states (Fig. 7c). It shows that for $\alpha < 1$, the generalized plane strain cases are qualitatively identical to the plane strain case discussed in Section 5. Lowering α narrows the gap between λ_{dry} and λ_{wet}. For $\alpha > 1$, however, λ_{dry} and λ_{wet} are flipped because the elongation of the surface feature is driven by a compressive stress state. For example, in the case of uniaxial deformation in x_3 ($\alpha = 2$), the elongation of the surface feature in x_1 is driven by the compression in x_3. Then Π decreases with λ_1, and more solvent is squeezed out as the surface features elongate.

8. The effect of stress-free amplitude: h_0/L_0

Under the assumption of shallow amplitude $h_0/L_0 \ll 1$, the elastocapillary effect is linear and $h(\lambda_1)/h_0$ is independent of h_0/L_0.[14] However, the osmocapillary effect is intrinsically nonlinear due to the moving boundaries of phase separation.[25] Consequently, $h(\lambda_1)/h_0$ is expected to show a strong dependence on h_0/L_0 for any amplitude in the presence osmocapillary phase separation. To illustrate this, we vary h_0/L_0 and simulate the evolution of h/h_0 for a purely elastocapillary case ($\gamma/\mu L_0 = 0.2$, $\gamma/\Pi_0 L_0 \ll 1$) and an osmocapillary case ($\gamma/\mu L_0 = 0.2$, $\gamma/\Pi_0 L_0 = 10$) under the plane strain condition and assume incompressible network. In the elastocapillary case (Fig. 8a), $h(\lambda_1)/h_0$ shows weak dependence on the amplitude h_0/L_0 when $h_0/L_0 < 1$. Yet, a large amplitude of $h_0/L_0 > 1$ is significantly harder to flatten. In the osmocapillary case (Fig. 8b), increasing h_0/L_0 significantly enhances the initial flattening (lower h/h_0 at $\lambda_1 = 1$) and delays the disappearance of osmocapillary phase separation at λ_{dry}. λ_{wet} is determined by setting $\Pi = 0$ in eqn (4), thus independent of amplitude h_0/L_0. The change in the initial flattening and λ_{dry} is significant even between the cases that have nearly identical elastocapillary behaviors ($h_0/L_0 = 0.02$ and 0.2). The strong amplitude dependence of osmocapillary phase separation is easy to understand (Fig. 8c): the competition between the osmotic and capillary effects dictates the surface radius of curvature to be the osmocapillary length γ/Π,[23] thus the larger the h_0/L_0, the larger the amount of osmocapillary phase separation, and thus the more difficult it is to dry the surface.

9. Conclusion

In this paper, we have performed systematic finite element analyses of how a sinusoidal surface deforms with stretch in the presence of the coupled elastocapillary and osmocapillary effects. When both the elastocapillary and osmocapillary effects are weak ($\gamma/\mu L_0 \ll 1$, $\gamma/\Pi_0 L_0 \ll 1$), the surface flattens with stretch due to the Poisson effect. Elastocapillary deformation alone can lead to surface roughening with stretching ($\gamma/\mu L_0 \sim 0.1$ or higher, $\gamma/\Pi_0 L_0 \ll 1$). However, such roughening is limited to relatively small deformation. For large tension and compression, the Poisson effect dominates over the capillary effect thus resuming the flattening. Osmocapillary phase separation also leads to surface roughening with stretching ($\gamma/\Pi_0 L_0 \sim 1$ or higher with any $\gamma/\mu L_0$). The osmocapillary roughening happens over a limited stretch range bounded by λ_{dry} and λ_{wet}. Outside this range, the surface is either dry, thus purely elastocapillary, or inundated under exuded solvent, thus completely flat. The range between λ_{dry} and λ_{wet} is strongly

affected by the out-of-plane constraint (λ_3) and the surface amplitude (h_0/L_0). In common loading conditions such as uniaxial and equibiaxial deformations, osmocapillary phase separation leads to much stronger stretching-dependent roughening than elastocapillary deformation. The richness of deformation-dependent gel surface topography can be used to design novel stimuli-responsive surfaces with tunable surface topography.

Conflicts of interest

There are no conflicts to declare.

References

1 B. N. Persson, Theory of rubber friction and contact mechanics, *J. Chem. Phys.*, 2001, **115**(8), 3840–3861.
2 D. E. Packham, Surface energy, surface topography and adhesion, *Int. J. Adhes. Adhes.*, 2003, **23**(6), 437–448.
3 K. Fuller and D. Tabor, The effect of surface roughness on the adhesion of elastic solids, *Proc. R. Soc. London, Ser. A*, 1975, **345**(1642), 327–342.
4 M. Ramiasa, *et al.*, The influence of topography on dynamic wetting, *Adv. Colloid Interface Sci.*, 2014, **206**, 275–293.
5 S. M. Lößlein, F. Mücklich and P. G. Grützmacher, Topography versus chemistry–How can we control surface wetting?, *J. Colloid Interface Sci.*, 2022, **609**, 645–656.
6 X. Yao, *et al.*, Adaptive fluid-infused porous films with tunable transparency and wettability, *Nat. Mater.*, 2013, **12**(6), 529–534.
7 Y. Lin, *et al.*, Surface roughness and light transmission of biaxially oriented polypropylene films, *Polym. Eng. Sci.*, 2007, **47**(10), 1658–1665.
8 L. Chen, *et al.*, Thermal-responsive hydrogel surface: tunable wettability and adhesion to oil at the water/solid interface, *Soft Matter*, 2010, **6**(12), 2708–2712.
9 D. Liu, *et al.*, (Photo-) thermally induced formation of dynamic surface topographies in polymer hydrogel networks, *Langmuir*, 2013, **29**(18), 5622–5629.
10 J. Comelles, *et al.*, Microfabrication of poly (acrylamide) hydrogels with independently controlled topography and stiffness, *Biofabrication*, 2020, **12**(2), 025023.
11 Y. Hu, J.-O. You and J. Aizenberg, Micropatterned hydrogel surface with high-aspect-ratio features for cell guidance and tissue growth, *ACS Appl. Mater. Interfaces*, 2016, **8**(34), 21939–21945.
12 J. Zhu, C. Yang and Q. Liu, Experimental characterization of elastocapillary and osmocapillary effects on multi-scale gel surface topography, *Soft Matter*, 2023, **19**(45), 8698–8705.
13 S. Zhao, *et al.*, Mechanical stretch for tunable wetting from topological PDMS film, *Soft Matter*, 2013, **9**(16), 4236–4240.
14 N. Bain, *et al.*, Surface tension and the strain-dependent topography of soft solids, *Phys. Rev. Lett.*, 2021, **127**(20), 208001.
15 S. C. Truxal, Y.-C. Tung and K. Kurabayashi, High-speed deformation of soft lithographic nanograting patterns for ultrasensitive optical spectroscopy, *Appl. Phys. Lett.*, 2008, **92**(5), 051116.
16 P. Goel, *et al.*, Mechanical strain induced wetting transitions between anisotropic and isotropic on polydimethylsiloxane (PDMS) films patterned by optical discs, *Appl. Surf. Sci.*, 2015, **356**, 102–109.
17 N. Lapinski, *et al.*, A surface with stress, extensional elasticity, and bending stiffness, *Soft Matter*, 2019, **15**(18), 3817–3827.
18 C.-Y. Hui, *et al.*, How surface stress transforms surface profiles and adhesion of rough elastic bodies, *Proc. R. Soc. A*, 2020, **476**(2243), 20200477.
19 B. Andreotti, *et al.*, Solid capillarity: when and how does surface tension deform soft solids?, *Soft Matter*, 2016, **12**(12), 2993–2996.
20 R. W. Style, *et al.*, Elastocapillarity: Surface tension and the mechanics of soft solids, *Annu. Rev. Condens. Matter Phys.*, 2017, **8**, 99–118.
21 D. Paretkar, *et al.*, Flattening of a patterned compliant solid by surface stress, *Soft Matter*, 2014, **10**(23), 4084–4090.
22 A. Jagota, D. Paretkar and A. Ghatak, Surface-tension-induced flattening of a nearly plane elastic solid, *Phys. Rev. E: Stat., Nonlinear, Soft Matter Phys.*, 2012, **85**(5), 051602.
23 Q. Liu and Z. Suo, Osmocapillary phase separation, *Extreme Mech. Lett.*, 2016, **7**, 27–33.
24 R. W. Style, *et al.*, The contact mechanics challenge: Tribology meets soft matter, *Soft Matter*, 2018, **14**(28), 5706–5709.
25 J. Zhu and Q. Liu, The osmocapillary effect on a rough gel surface, *J. Mech. Phys. Solids*, 2023, **170**, 105124.
26 M. Rubinstein and S. Panyukov, Elasticity of polymer networks, *Macromolecules*, 2002, **35**(17), 6670–6686.
27 A. Chakrabarti and M. K. Chaudhury, Direct measurement of the surface tension of a soft elastic hydrogel: exploration of elastocapillary instability in adhesion, *Langmuir*, 2013, **29**(23), 6926–6935.
28 M. Quesada-Pérez, *et al.*, Gel swelling theories: the classical formalism and recent approaches, *Soft Matter*, 2011, **7**(22), 10536–10547.
29 W. Hong, *et al.*, A theory of coupled diffusion and large deformation in polymeric gels, *J. Mech. Phys. Solids*, 2008, **56**(5), 1779–1793.
30 W. Hong, X. Zhao and Z. Suo, Formation of creases on the surfaces of elastomers and gels, *Appl. Phys. Lett.*, 2009, **95**(11), 111901.
31 Q. Liu, *et al.*, Elastocapillary crease, *Phys. Rev. Lett.*, 2019, **122**(9), 098003.
32 J. Li, *et al.*, Experimental determination of equations of state for ideal elastomeric gels, *Soft Matter*, 2012, **8**(31), 8121–8128.
33 Q. Xu, *et al.*, Direct measurement of strain-dependent solid surface stress, *Nat. Commun.*, 2017, **8**(1), 555.
34 Q. Xu, R. W. Style and E. R. Dufresne, Surface elastic constants of a soft solid, *Soft Matter*, 2018, **14**(6), 916–920.
35 X. Guan, *et al.*, Rate-dependent creasing of a viscoelastic liquid, *Extreme Mech. Lett.*, 2022, **55**, 101784.

36 Y. Hu, *et al.*, Using indentation to characterize the poroelasticity of gels, *Appl. Phys. Lett.*, 2010, **96**(12), 121904.
37 Y. Hu, *et al.*, Indentation of polydimethylsiloxane submerged in organic solvents, *J. Mater. Res.*, 2011, **26**(6), 785–795.
38 S. Cai, *et al.*, Poroelasticity of a covalently crosslinked alginate hydrogel under compression, *J. Appl. Phys.*, 2010, **108**(11), 113514.
39 Y. Hu, *et al.*, Poroelastic relaxation indentation of thin layers of gels, *J. Appl. Phys.*, 2011, **110**(8), 086103.
40 Z. Shao and Q. Lin, Independent characterization of the elastic and the mixing parts of hydrogel osmotic pressure, *Extreme Mech. Lett.*, 2023, **64**, 102085.
41 A. N. Gent, *Engineering with rubber: how to design rubber components*, Carl Hanser Verlag GmbH Co KG, 2012.

